Analyzing the extent and use of impervious land in rural landscapes

Journal Article

Author(s):
Moser, Andreas; Van Vliet, Jasper; Wissen Hayek, Ulrike; Grêt-Regamey, Adrienne

Publication date:
2024-12

Permanent link:
https://doi.org/https://doi.org/10.3929/ethz-b-000694898

Originally published in:
Geography and Sustainability 5(4), https://doi.org/10.1016/j.geosus.2024.08.004

Geography and Sustainability 5 (2024) 625–636

Contents lists available at ScienceDirect

Geography and Sustainability

journal homepage: www.elsevier.com/locate/geosus

Research Article

Analyzing the extent and use of impervious land in rural landscapes

Andreas Moser[a,*], Jasper van Vliet[b], Ulrike Wissen Hayek[a], Adrienne Grêt-Regamey[a]

[a] Planning of Landscape and Urban Systems (PLUS), ETH Zurich, Stefano-Franscini-Platz 5, Zurich, Switzerland
[b] Institute for Environmental Studies (IVM), Vrije Universiteit Amsterdam, De Boelelaan 1111, Amsterdam, the Netherlands

HIGHLIGHTS

- Rural and urban areas have similar extent of impervious land cover.
- Rural impervious surfaces are mainly for transport infrastructure and agriculture.
- CNNs on orthophotos were successful for building type classification.
- Land policies for rural development should consider the impervious land use.

GRAPHICAL ABSTRACT

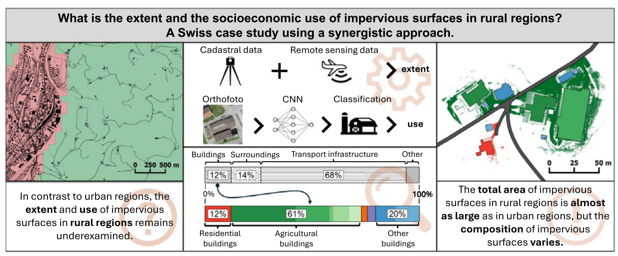

ARTICLE INFO

Article history:
Received 22 May 2024
Received in revised form 22 August 2024
Accepted 23 August 2024
Available online 3 September 2024

Keywords:
Soil sealing
Rural areas
Very-high-resolution aerial imagery
Building types
Convolutional neural networks
Cadastral data

ABSTRACT

The amount of impervious surface is increasing rapidly worldwide. Although urban expansion has been studied extensively, the alteration of impervious land cover in rural regions remains under-examined. In particular, insights into the utilization of these sealed surfaces are crucially needed to unravel the underlying dynamics of land use changes beyond urban areas. This study focuses on rural regions from a Swiss case study and presents an analysis of the *use* of sealed surfaces in such regions, rather than solely quantifying the *extent* of sealed surfaces. Utilizing a synergistic approach that merges detailed cadastral plans with very-high-resolution remote sensing imagery and sophisticated deep learning algorithms, we characterized the uses of sealed surfaces, including buildings and their surroundings. Our findings reveal that 2.1 % of the study area's rural regions comprises sealed surfaces - an area comparable to the sealed surfaces in the urban regions. Within these rural regions, transport infrastructure represents 68 % of this impervious surface. Buildings account for 12 %, and their surroundings, constituting 13 %, are utilized primarily for agricultural purposes, including farming and livestock activities. The deep learning approach achieved a classification accuracy of 72 % for a shallow model and 79 % for a deeper model, indicating that mapping building types is possible with reasonable accuracy. The outcomes of this study underscore the critical need to factor in the presence and utilization of impervious land cover within rural regions for the sustainable management of land resources.

1. Introduction

Impervious land cover is expanding worldwide at unprecedented rates (Liu et al., 2020). Forecasts by Gao and O'Neill (2020) indicate a potential increase in global impervious areas by a factor of 1.8 to 5.9 throughout the 21st century. The conversion of natural into impervious land, also referred to as soil sealing, poses a major threat to soils (Stolte et al., 2015) with effects on soil processes, i.e., energy transfer, water movement, gas diffusion, and biota (Scalenghe and Marsan, 2009) and its ecosystem services, e.g., food provisioning, biodiversity conservation, climate regulation, and recreation services (Baveye et al., 2016). Particularly in rural regions, this irreversible process adversely affects sensitive scenic landscapes with cultural heritage and high biodiversity value, leading to fragmentation and a loss of landscape identity (Antrop, 2000). However, previous studies predominantly have focused on urban environments (Ravetz et al., 2013). The expansion of impervious land cover extends far beyond urban settings, with rural regions exhibiting a diverse array of small-scale mosaics comprising residential, agricultural, commercial, or industrial uses, alongside significant infrastructure. These regions are undergoing a diffusive urbanization

* Corresponding author at: ETH Zürich - Planning of Landscape and Urban Systems (PLUS), Stefano-Franscini-Platz 5, HIL H 41.2, 8093 Zürich, Switzerland.
E-mail addresses: moserandreas@ethz.ch (A. Moser), jasper.van.vliet@vu.nl (J. van Vliet), ulrike.wissen@ethz.ch (U. Wissen Hayek), gret@ethz.ch (A. Grêt-Regamey).

https://doi.org/10.1016/j.geosus.2024.08.004

process related to various cultural and socioeconomic changes that are transforming the traditional countryside into a complex and multifunctional landscape (Antrop, 2004; Shaw et al., 2020). Nonetheless, the extent and specific uses of sealed surfaces in rural settings remain largely unquantified. Such information is imperative for devising strategies to safeguard fertile soils, prevent landscape fragmentation, protect natural landscapes, and enhance ecosystem service provision. In fact, sustainable soil management is pivotal for advancing the Sustainable Development Goals (SDGs) of the United Nations (Lal et al., 2021; UN General Assembly, 2015). With regard to achieving the European Commission's objective of net zero land take by 2050 (European Commission, 2011), such data will be needed to assess of various initiatives' performance and to monitor the process.

With the emergence of high-resolution satellite imagery (defined by a spatial resolution of < 10 m) at the turn of the millennium, a wide range of mapping applications and methods for assessing impervious land cover have been developed (Peroni et al., 2022; Wang and Li, 2019; Weng, 2012). Numerous multi-temporal impervious land cover products exist with relatively high spatial resolution at pan-European (CLMS, 2020; EEA, 2018) or global levels (Li et al., 2020; Liu et al., 2018; Pesaresi et al., 2016). However, even at high resolutions, raster-based data overlook small-scale sealed surfaces in rural regions. In addition, to address the challenges described above, data is needed that includes both the physical extent and socioeconomic uses of the land (Hersperger et al., 2018).

In recent years, there have been considerable advances in mapping land use activities in urban regions, mostly machine learning and deep learning algorithms (Yin et al., 2021; Zhu et al., 2017). In particular, convolutional neural networks (CNNs) have been shown to excel at computer vision tasks (Alzubaidi et al., 2021) and have been employed in remote sensing for various land cover and land use classification tasks using satellite and aerial imagery (Ma et al., 2019). For instance, CNNs were used for impervious land use classification in urban regions at the level of pixels (Chen et al., 2016; Yue et al., 2015), objects (Yoo et al., 2022; Zhang et al., 2018; Zhao et al., 2017), and scenes (Albert et al., 2017; Chen et al., 2021). To address the problem of mixed uses within such areal classification of urban land, models were proposed at the individual building level. Kang et al. (2018) developed a framework for classifying building types using ground-based street views, Srivastava et al. (2020) complemented such an approach with interior views of buildings, and Hoffmann et al. (2019) mapped building types using both aerial and street view images.

This paper aims to quantify sealed surfaces and assess their use in rural regions in a case study of Switzerland, contributing to the general knowledge of impervious land use in rural landscapes. The research objectives include determining the extent of buildings, impervious surfaces around buildings and transport infrastructure, and in particular ascertaining these surfaces' socioeconomic purposes. In addition, we demonstrate the effectiveness of automated building type classification using deep learning techniques for impervious land use identification. The validity of the resulting extent and use of impervious land is evaluated by comparing our findings with available raster data. Our study is centered around the Canton of Bern in Switzerland, a country known for its significant degree of imperviousness, with 2.8 % sealed surface, ranking it ninth out of 39 European countries according to the European Environment Agency (EEA, 2020), and making it a pertinent case study. The paper concludes by discussing the significance of soil sealing in rural regions to the overall impervious land cover, and its implications for understanding and directing drivers of land use change.

2. Materials and methods

2.1. Study area

Switzerland is located at the center of Europe and accommodates a population of 8.7 million with a relatively high average density of 212 inhabitants/km^2 (FSO, 2022a), compared with 109 inhabitants/km^2 on average in the European Union (Eurostat, 2022). In a study by Hennig et al. (2015), Switzerland ranked in the upper tercile in terms of urban sprawl among European countries. Urban sprawl, understood by Hennig et al. (2015) as spatially dispersed urban development with low intensity of use, affects large parts of Europe, and is pronounced in the vicinity of urban centers, along transportation corridors, and in industrialized regions.

Like many other countries in Europe, Switzerland has implemented urban growth boundaries, i.e., building zones to contain urban sprawl, and promotes densification of already built areas (Gerber et al., 2018). Building zones hold 95 % of the population on just 5 % of the country's territory (ARE, 2022). The Swiss Spatial Planning Act restricts construction outside of building zones, only allowing renovation or construction of new agricultural buildings (*Swiss Federal Act on Spatial Planning*, 1979). However, some exemptions are related to existing buildings, as well as site-specific new constructions and infrastructure, such as roads, quarries, or buildings for energy production. Despite the containment strategy and a recent trend towards densification, 36 % of the country's artificial surfaces and 19 % of its building area are located outside of building zones with an increasing trend (ARE, 2023). The Canton of Bern is the second largest Swiss canton in terms of inhabitants (1 million in 2021) and area (5,959 km^2) out of 26 cantons, and it hosts the federal capital Bern itself with 134 thousand inhabitants (FSO, 2022a). Building zones in the study area span over 263 km^2 and include residential, public, touristic, artisanal, or industrial urban development, but not transport infrastructure (ARE, 2022). According to cantonal cadastral data, the landscape is predominantly agricultural, with 2,605 km^2 designated as arable land and alpine pastures. Forested areas cover 1,864 km^2, while 664 km^2 are natural areas without vegetation, such as rock, scree, or glaciers. In addition, water bodies cover 75 km^2 of the landscape.

2.2. Methodology overview

In this paper, we defined *rural regions* as areas outside of building zones (refer to Fig. 1). Using a grid resolution of 100 m × 100 m, we designated all grid cells intersecting with the building zones as urban, covering 9 % or 555 km^2, thereby delineating the extent of the rural regions, spanning 5,404 km^2 and covering approximately 91 % of the Canton of Bern.

The approach to extract and characterize soil sealing encompasses several steps (Fig. 2). In an initial step, we extracted all impervious surfaces in the Canton of Bern from the cadastral data, including buildings, transport infrastructure, and other impervious surfaces such as quarries and landfill sites. However, beyond these land cover classes, the entries in the cadastral database do not allow for identifying sealed surfaces surrounding buildings.

We then used very-high-resolution multispectral aerial imagery to assess the extent of the impervious surface surrounding these buildings, such as driveways, parking lots, or patios. We assumed that impervious surfaces around buildings occur within a maximal distance of 20 m. This perimeter is independent of building size but tends to be smaller for detached alpine huts and barns. Thus, we used 20 m buffers (10 m for alpine huts and barns) around buildings clipped with the land parcel boundaries for detection of impervious surfaces around buildings. The parsimonious normalized difference vegetation index (NDVI) threshold approach was applied to the high resolution multispectral orthophotos (SWISSIMAGE RS) to map sealed soils in the buffered area around buildings. The threshold of the NDVI value for impervious surfaces was set at 0.1 or lower (Defries and Townshend, 1994). Comprehensive mapping of the impervious land cover extent was conducted across the entire study area and compared between urban and rural regions to assess the prevalence of impervious surfaces. We compared the land cover extent mapping results with the raster-based land cover product of impervi-

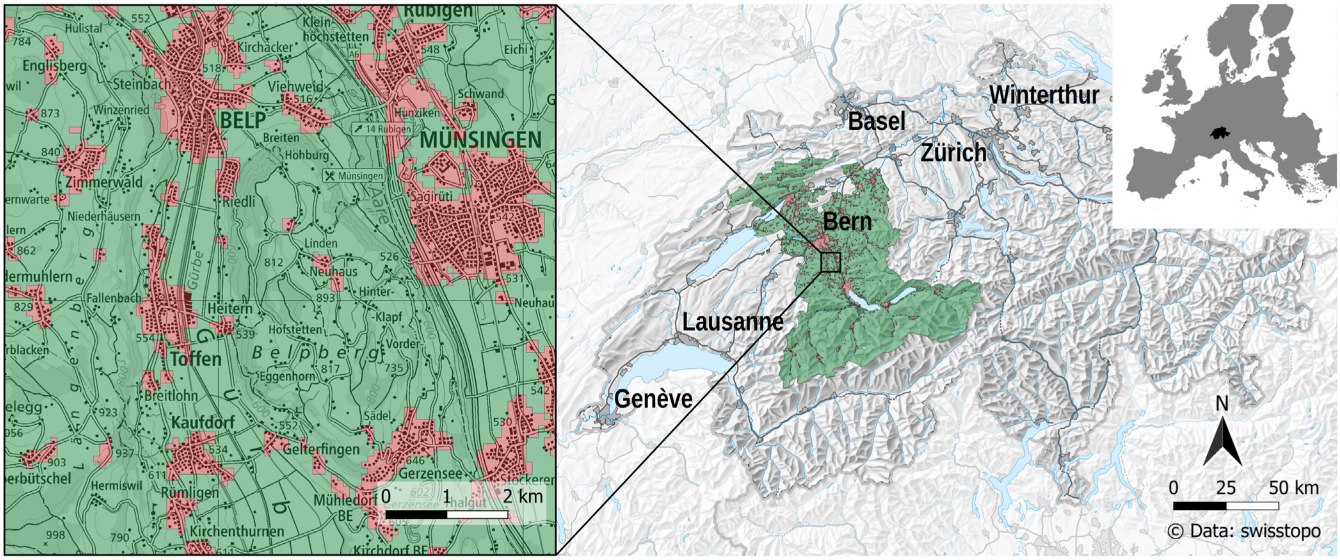

Fig. 1. The study area with zoomed in example illustrating rural regions (green) and urban regions (red) of the Canton of Bern in Switzerland.

Table 1
Classification scheme of impervious land cover and land use categories used in this study.

Impervious land cover	Land use	Data
Buildings	Residential Agricultural Commercial Industrial Other	Cadastral data, SWISSIMAGE 10 cm (RGB)
Surfaces around buildings	Residential Agricultural Commercial Industrial Other	Cadastral data, SWISSIMAGE 10 cm (RGB), SWISSIMAGE RS (RGB and NIR)
Transport infrastructure	Roads Railways Airfields	Cadastral data
Other impervious surfaces	Quarries and landfill	Cadastral data

ousness density from the European Union's Copernicus Land Monitoring Service (CLMS, 2020).

Finally, we mapped the use of the sealed surfaces by classifying building types using a shallow and deep convolutional neural network applied to very-high-resolution aerial imagery (see Section 2.4). The results were compared with a raster-based land use dataset in terms of land cover class agreement and raster overlay (see Section 2.5).

2.3. Data sources

Cadastral data was used to extract surfaces of impervious land cover from buildings, transport infrastructure, and other impervious surfaces (cf. Table 1). The vector data from 2021 covers the entire study area and maps buildings, transport infrastructure, and other impervious surfaces with high precision (KKVA, 2011).

To identify the use of impervious land cover, we used very-high-resolution orthoimages and deep learning models. On one hand, the buildings were classified using the product SWISSIMAGE 10 cm (Swisstopo, 2021a) to extract very-high-resolution orthoimages (RGB) without distortions of buildings. On the other hand, the Federal register of buildings and dwellings (RBD) of the Swiss Federal Statistical Office (FSO, 2022b) was used to generate labeled data for training the deep learning models for the building type classification. The RBD contains essential administrative data of nearly all buildings in Switzerland and identifies their main use. Their classification follows the Eurostat classification of types of constructions (CC) (Eurostat, 1998) with few modifications regarding restaurants and agricultural buildings.

For mapping impervious surfaces around buildings, very-high-resolution multispectral orthophotos from the Swiss Federal Office of Topography (Swisstopo, 2021b) were used. The multispectral images SWISSIMAGE RS (RGB and NIR) have a ground resolution of 0.1 m in flat areas and 0.25 m in mountainous areas. The fly-over dates of 2020 and 2021 during late summer were used, covering the entire study area. This image data was derived from the same flights and camera as the SWISSIMAGE 10 cm imagery, but unlike the latter, it was not post-processed with respect to overlaps and manual radiometric and geometric corrections. In addition, parcels from the cadastral data delineating land ownership were used to map the land use of impervious surfaces around buildings based on building types.

2.4. Mapping the impervious land use

2.4.1. Image retrieval and preprocessing for building type classification

We used deep learning algorithms to identify the use of buildings based on orthorectified very-high-resolution images. The visual differences of building types from a bird's-eye view include size, shape, and roof structure, including the roof's color, texture, material, and prominent features (e.g., balconies, light inlets, ventilation systems). Equally important to the visual distinction of the building types are surrounding areas with driveways, garden landscaping, vehicles, and agricultural or residential properties.

Square images of all buildings in the study area were retrieved from the SWISSIMAGE 10 cm orthophotos with a size of 600 × 600 pixels (see examples in Supplementary Material Fig. S1). Buildings smaller than 75 m^2 were excluded from the building type classification due to indistinct use, missing visual features, and loss of quality when upscaled to the input image size (600 × 600 pixels). Starting with the minimal square bounding box enclosing the building footprint of the cadastral survey, retrieval was conducted by adding 30 % of padding. Scaled padding ensures that the image captures the immediate surrounding area with distinct visual features.

Supervised learning of neural networks requires a large set of labeled data, including inputs and correct outputs. Labelling images with the correct building type for a training set was realized with an automatic step followed by manual curation. In Switzerland, each building is assigned a unique identifier in the cadastral data that allows it to be

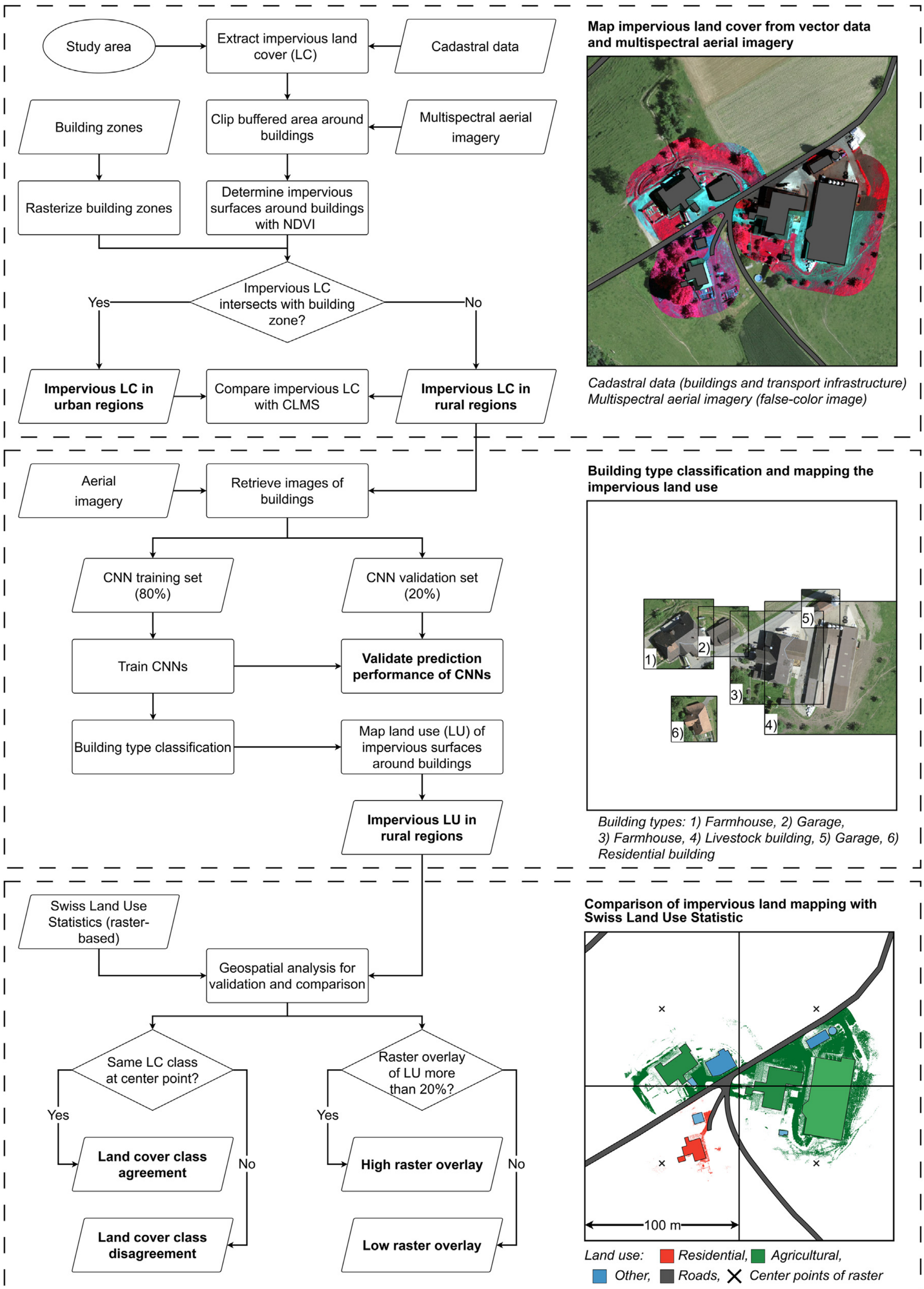

Fig. 2. Overview of the methodology to extract and characterize impervious land cover and land use in the study area.

Table 2
Description of building types per land use class.

Land use	Building type	Description	Frequent visual features	Number of samples
Residential	Residential building	Building for residential purposes with one or more dwellings	Gardens, patios, trampolines, pools, dormer windows, chimneys, moderate size, square shape	1,826
Agricultural	Farmhouse	Building for mixed residential and agricultural purpose	Residential features (gardens, patios, etc.), livestock features (hay bales, light inlets, animals, etc.), farm environment, large size, intersecting gables, and hip roofs	1,881
	Livestock building	Building for animal husbandry	Hay bales, animals, animal outlet sites, light inlets, ventilation systems, rectangular shape, gable roofs	1,062
	Greenhouse	Building for protected cultivation	White or transparent roofs, large size, rectangular shape	124
	Barn	Building for undefined agricultural purposes (mostly storage)	Detached in field, small access roads, small size, square-shaped, gable roofs	1,504
	Alpine hut	Building for shelter and storage, for alpine farming purposes	Detached in rugged alpine environment, footpaths, tin roofs	1,810
Commercial	Hospitality building	Restaurants and hotels	Terraces, parasols	122
Industrial	Industrial building	Factory building, gravel plant, electricity production or similar	Parking lots, trucks, gravel sites, logs	305
Other	Garage	Building for storage of motor vehicles, machinery or equipment	Annex buildings, driveways, cars, machinery, flat or saltbox roofs	1,187
	Other building (< 75 m^2)	Miscellaneous building with footprint smaller than 75 m^2 that was not classified using CNN		–

linked to the RBD. The RBD's building types were grouped into the nine building types defined in this study (cf. Table 2). However, manual curation was indispensable because the RBD does not distinguish buildings with mixed usage (e.g., farmhouses), agricultural buildings are not categorized in more detail (e.g., greenhouses, barns, alpine huts, etc.), and the register's data quality is generally questionable due to incorrect labels. The curated data was only used to generate training and validation data for the deep learning model to ensure a transferable method to regions without such extensive building data. The category *other* includes buildings from the impervious land cover map that were not classified due to their small size (cf. Table 2). Building types with insufficient occurrence (<100) in rural regions were excluded from the training of the classification models.

The training data comprised 9,821 images distributed unevenly across the nine building types (Table 2) and was split randomly, with a ratio of 80:20 for training and testing, respectively. Using data augmentation techniques, the training set was increased artificially with a random rotation and random horizontal flip (Taylor and Nitschke, 2018). Finally, the images' RGB channel values were rescaled to the range of [0, 1] to enhance robustness with respect to lighting conditions and color balance (Géron, 2019).

2.4.2. Building type classification with convolutional neural networks

Classification of building types was conducted with CNNs. In contrast to other machine learning algorithms, CNNs combine feature learning and classification by expressing the probability of an image belonging to a particular class. Feature learning in neural networks occurs in a series of hidden layers of different types. At the core of this pipeline are convolutional layers, in which the input image is convolved with a collection of filters or kernels, creating feature maps. Feature maps are typically passed through an activation function (e.g., rectified linear units, ReLU) to introduce non-linearity to the network and enable learning of complex non-linear relationships between input and output. Pooling layers (e.g., max pooling) reduce the spatial dimensions of feature maps and makes the network translation invariant, i.e., objects are recognized regardless of their relative position in the image. This downsampling technique also acts as a form of regularization to prevent overfitting and makes the network computationally more efficient, reducing parameters while retaining the dominant information in the feature maps. Other commonly used layers in feature learning are batch normalization to improve stability and speed of the training process, and dropouts, in which randomly, a fraction of neurons is removed during training to prevent overfitting. The classification prediction is achieved at the end of the network with a fully connected layer based on the extracted features from the convolutional and pooling layers. This layer's input is created by flattening the previous feature map into the form of a vector. The number of neurons in this layer equals the number of classes in a classification task. In the case of multiclass problems, the last fully connected layer is commonly activated with a softmax function transforming the output to a probability distribution of scores per class (Alzubaidi et al., 2021; Géron, 2019).

We used both a Shallow Convolutional Neural Network (SCNN) with reduced training costs and a deep convolutional neural network (Xception) optimizing the error rate on the training dataset. The advantages of a shallow convolutional neural network architecture are low implementation complexity, fast learning, and reduced computational resources due to fewer parameters and calculations in the shorter pipeline of hidden layers (Kim et al., 2021; Miao et al., 2019). Nevertheless, they have been proven to perform well on popular benchmark databases (Lei et al., 2020; McDonnell and Vladusich, 2015). In contrast, deep neural networks with large numbers of layers are more effective at learning complex high-level features, and network architectures such as AlexNet (Krizhevsky et al., 2012), VGGNet (Simonyan and Zisserman, 2014), ResNet (He et al., 2016), or Xception (Chollet, 2017) achieved some of the lowest error rates at the ImageNet Large Scale Visual Recognition Challenge (ILSVRC).

The model structure of the SCNN used in this study (cf. Fig. S2) was designed similar to the network architecture proposed by Lei et al. (2020). The input image ($600 \times 600 \times 3$) was passed to three successive building blocks consisting of a convolutional layer (with 16, 32, and 64 kernels of size 3×3), a batch normalization, an activation layer (ReLU), and a pooling layer (max pooling with window size 3×3 and stride 2). A dropout layer with a rate of 0.3 was applied before flattening for the fully connected layer with a softmax activation.

The Xception model (cf. Fig. S3) was used as a state-of-the-art deep neural network to opt for a more efficient feature extraction and high-level characteristics. The model is a variant of the Inception models (Ioffe and Szegedy, 2015; Szegedy et al., 2017, 2015), involving depthwise separable convolution (i.e., convolution that applies a separate filter to each input channel) to reduce computational expense. The architecture stacks 36 convolutional layers and uses residual connections to improve the training. The model was adapted with a dropout layer with a rate of 0.5 before the fully connected layer for better generalization.

For both CNN models, the hyperparameters were set according to standard computer vision procedures. The Adam optimizer (Kingma and Ba, 2014) with a learning rate of 1e-3 was used, the number of epochs was set to 300, and the batch size was 8 for SCNN and 4 for Xception to overcome the problem of resource exhaustion. The loss between labels and predictions was calculated using a cross-entropy function adjusted for the imbalanced dataset with weights derived from the number of samples per class.

2.4.3. Validation of convolutional neural network models

We used precision, recall, F1 scores, overall accuracy, and confusion matrix to evaluate the efficiency of the created building type classification models SCNN and Xception. The prediction performance was assessed using the test dataset (N = 1964), which is a holdout sample of 20 % of the training dataset (N = 9821). The model's accuracy was calculated by dividing the number of correct predictions by the total number of predictions made. A per-class measure of precision and robustness is the F1 score, which is the harmonic mean of precision and recall, as follows (van Rijsbergen, 1979):

$$\mathrm{F1} = 2 \times \frac{\mathrm{precision} \times \mathrm{recall}}{\mathrm{precision} + \mathrm{recall}} = \frac{\mathrm{tp}}{\mathrm{tp} + \frac{1}{2}\mathrm{fp} + \mathrm{fn}} \tag{1}$$

Precision measures the proportion of true positives (tp) out of all positive predictions for a class, i.e., the sum of tp and false positives (fp). Recall, also called sensitivity, measures the fraction of tp out of all actual positive predictions, i.e., the sum of fp and false negatives (fn). The macro and weighted averages over all classes were calculated as an overall evaluation metric. The macro average is the arithmetic mean of the per class F1 scores and the weighted average considers class support (number of elements in class) to account for imbalanced datasets.

A holistic view of the predictions is shown with the normalized confusion matrix. On each row, the matrix compares actual class values with the predicted class value normalized by the total number of samples.

2.4.4. Mapping building types and land use of impervious surfaces around buildings

After training and validation of the SCNN and Xception models, we selected the most accurate model to map all buildings in the study area. While we used multiple metrics for accuracy assessment, this selection was based on weighted average of F1 scores. In accordance with this criterion, the Xception model was ultimately used to map all buildings.

The land use of impervious surfaces around buildings was determined for each land parcel and inferred from the building types present on a given parcel. The following rules were used to determine land use: (1) *residential*, if there is at least one residential building and no farmhouse, livestock building, greenhouse, industrial or hospitality building; (2) *agricultural*, if there is a farmhouse, livestock building or greenhouse, or if there is only alpine huts and barns; (3) *industrial*, if there is an industrial building and no farmhouse, livestock building or greenhouse; (4) *commercial*, if there is a hospitality building and no farmhouse, livestock building or greenhouse; (5) *other*, if there is only a garage or a smaller building (other buildings < 75 m^2 are not classified with the CNN). We did not further specify land uses according to the types of buildings, as impervious surfaces around buildings cannot be attributed to a single building, except for stand-alone buildings.

2.5. Comparison of impervious land mapping with Swiss Land Use Statistic

The impervious land cover and land use map was compared with the raster-based Swiss Land Use Statistics collected from 2013 to 2018 and published 2019 by the Swiss Federal Statistical Office (FSO, 2019). Land cover and land use were collected separately, generating two codes per sample point, which can be evaluated both individually or in combination. The inventory comprises 27 land cover classes and 46 land use classes, which can be combined into 72 base categories. The map has a spatial resolution of 1 ha per raster cell, in which land cover and land use were interpreted at the center point. Swiss Land Use Statistics interpret land use by the integrity of a built-up site, so land use of buildings was determined in an aggregated way over the land parcels, analogous to the surfaces around buildings (see Section 2.4.4). The comprehensive land cover and land use classification of the Swiss Land Use Statistics allowed for a direct comparison between all classes, including impervious surfaces around buildings. Only the land use class *commercial* was combined with *other* because the Swiss Land Use Statistics does not specify this class separately.

To understand the influence of small-scale structures of impervious surfaces in rural regions on total areas of raster-based datasets, we compared the impervious land cover map in this study with the Swiss Land Use Statistics. For the comparison, we distinguished impervious land cover areas within raster cells of the Swiss Land Use Statistics based on the *land cover class agreement*, i.e., impervious areas within pixels of the corresponding land cover class, and the *raster overlay*, i.e., a *high* raster overlay means that the pixel has >20 % impervious land cover area, and a *low* raster overlay means that >80 % of the land cover is of another land cover class.

3. Results

3.1. Impervious land cover and land use in rural regions

Total impervious land cover in rural regions is 113.2 km^2, corresponding to 1.9 % of the Canton of Bern, or 2.1 % of rural regions within the canton. Transport infrastructure comprises the greatest share of impervious land cover, accounting for 68 % (76.7 km^2), of which 95 % is roads, 4 % is railways, and 1 % is airfields (Fig. 3). Building footprints occupy 12 % (13.9 km^2), and the surfaces around buildings are even larger, occupying 14 % (15.7 km^2). Other impervious surfaces, i.e., quarries and landfill sites, cover 6.9 km^2, or 6 % of the total impervious land cover. By comparison, total impervious land cover in urban regions amounts to 154.6 km^2, or 2.6 % of the total study area. The sealed surface within urban regions comprises 34.0 % (52.5 km^2) building area, 32.0 % (49.5 km^2) surfaces around buildings, 33.3 % (51.5 km^2) transport infrastructure, and 0.7 % (1.1 km^2) other impervious surfaces.

Most of the building area in rural regions is used for agriculture. Farmhouses make up 30 % of the building area, 16 % are used for livestock buildings, 7 % for barns, another 6 % are used for alpine huts, and 2 % for greenhouses. Altogether, agricultural uses account for 61 % of the building area, covering 8.5 km^2. By comparison, residential buildings occupy an area of 1.7 km^2 and account for 12 % of all building areas. The share of hospitality and industrial buildings is even lower, covering only 3 % and 4 % of the building area, respectively. Not negligible are building areas of garages and other buildings with a footprint smaller than 75 m^2. Garages cover 9 % (1.3 km^2) and other buildings 11 % (1.5 km^2) of the building area.

Impervious surfaces around buildings are largely proportional to the building areas. Agricultural impervious surfaces around buildings are 11.36 km^2 and make up 72 % of all impervious surfaces around buildings. Evidently, agricultural impervious surfaces around buildings include surfaces around some garages, other smaller buildings, and even residential buildings, as land use is inferred from existing building types at the level of land parcels (cf. Section 2.4.4). Impervious surfaces around residential buildings cover 1.73 km^2 (11 % of all impervious surfaces around buildings) and have almost the same extent as the residential building area. Hospitality and industrial buildings are surrounded by impervious surfaces of 5.61 km^2 and 8.89 km^2, which is about 50 % larger than the building areas itself. In contrast, impervious surfaces around buildings for other land uses are relatively small. With an area of only 1.13 km^2, this is half the size of the respective building areas of both garages and other buildings combined. Two possible reasons may account for this result. First, garages are often part of a building complex in which other building types determine land use. Second, small buildings, such as garages or other buildings (with a footprint < 75 m^2 in this

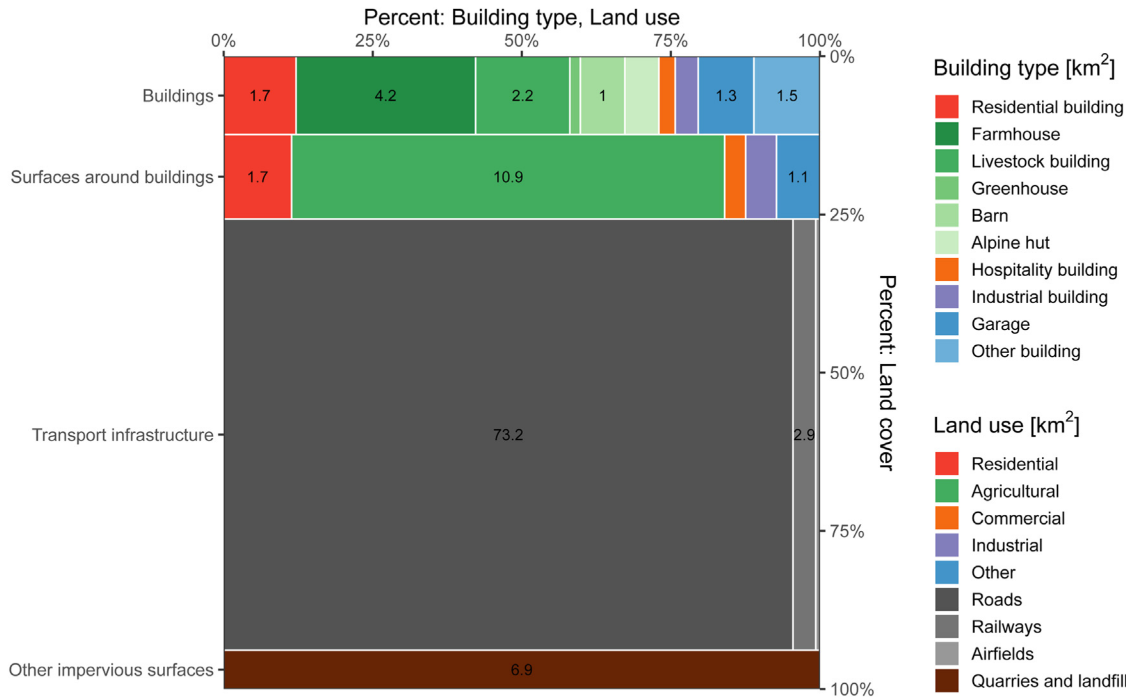

Fig. 3. Impervious land cover and land use in the case study area's rural regions. The land cover of buildings is represented by the building types with colors corresponding to land use.

Table 3
Per class precision, recall, and F1 score and macro average, weighted average, and overall accuracy for building type classification.

	SCNN			Xception			
Class	Precision	Recall	F1 score	Precision	Recall	F1 score	Support
Residential b.	0.91	0.65	0.75	0.92	0.79	0.85	364
Farmhouse	0.72	0.91	0.8	0.83	0.9	0.86	352
Livestock b.	0.55	0.69	0.61	0.7	0.75	0.72	224
Greenhouse	0.8	0.91	0.85	0.87	0.91	0.89	22
Barn	0.81	0.6	0.69	0.76	0.69	0.72	308
Alpine hut	0.76	0.79	0.78	0.8	0.78	0.79	377
Hospitality b.	0.35	0.62	0.45	0.43	0.76	0.55	21
Industrial b.	0.53	0.52	0.53	0.64	0.74	0.69	61
Garage	0.65	0.66	0.66	0.72	0.8	0.76	235
Macro avg. F1	0.68	0.7	0.68	0.74	0.79	0.76	1,964
Weighted avg. F1	0.74	0.72	0.72	0.79	0.79	0.79	1,964
Overall accuracy			0.72			0.79	1,964

study), are isolated from access roads and, therefore, from impervious soils.

The exact areas in square meters and percentages for all land cover, land use, and building types are provided in Tables S1 and S2, and are summarized in Fig. 3.

3.2. Building type classification with CNN

Classification of the nine building types of the test dataset with 1964 samples is achieved with an accuracy of 72 % using the SCNN model and 79 % using the Xception model, as presented in Table 3.

The Xception model showed signs of overfitting during training, with a continued increase in training accuracy but a stable validation accuracy. Presumably, high model complexity coupled with a relatively small training dataset causes the model to learn noise in the data and not generalizing well anymore. Therefore, an early stop of the model after 150 epochs is adopted as a regularization technique. Loss and accuracy curves for the training and validation datasets, illustrating the model's performance during training, are provided for both the SCNN and Xception models in Figs. S4 – S9.

Since the training dataset is highly imbalanced, the weighted averages are best suited for an overall assessment of the model performance respecting the number of instances per class. The models perform with a weighted average of F1 scores of 72 % for SCNN and 79 % for Xception. The deep neural network Xception improves the weighted average precision and recall scores by 5 % and 7 %, respectively, compared to SCNN, indicating that the model identifies more positive instances correctly and that it has a lower rate of false positives, respectively.

The differences in performance between the classes are similar with the two models. The highest F1 scores, i.e., the lowest overall false positives and false negatives, are achieved for the classes of greenhouses (85 % with SCNN, 89 % with Xception), farmhouses (80 % with SCNN, 86 % with Xception), and alpine huts (78 %) with SCNN, and residential buildings (85 %) with Xception. The lowest scores, especially because of low precision, are obtained for industrial buildings (53 % with SCNN, 69 % with Xception) and hospitality buildings (45 % with SCNN, 55 % with Xception) classes. Both classes have a low number of supports. For

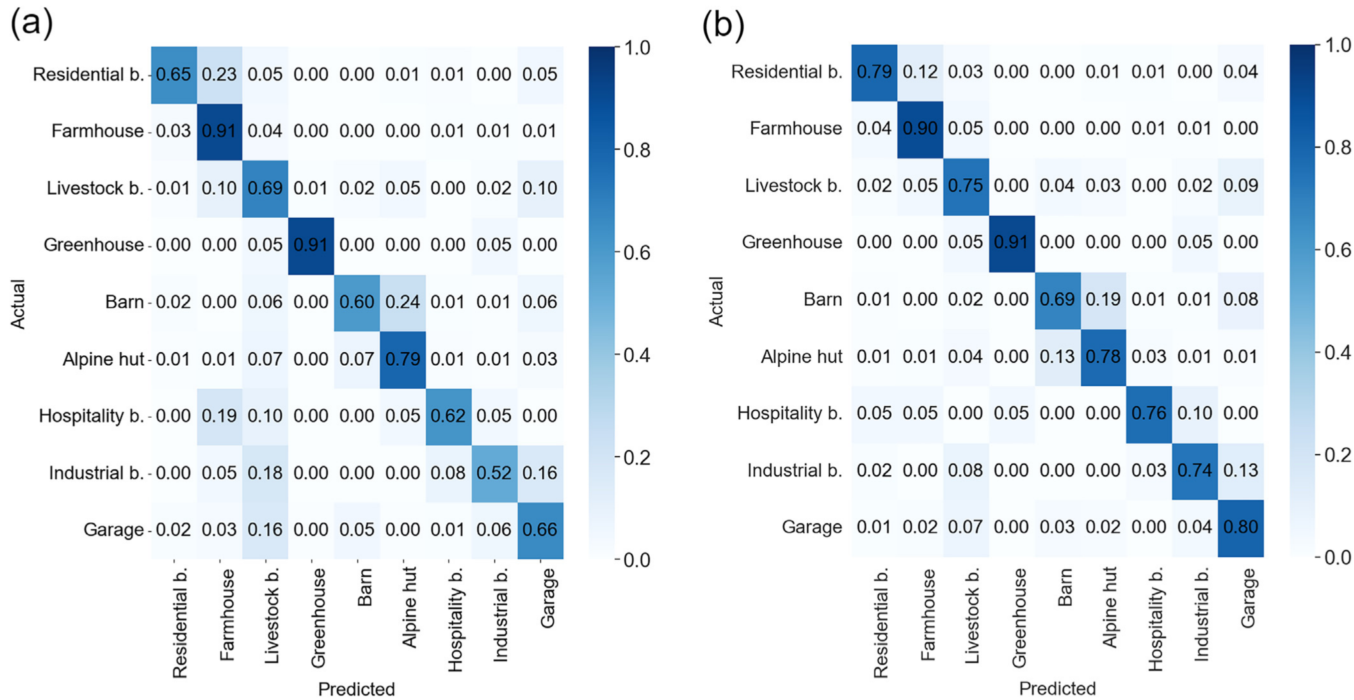

Fig. 4. Normalized confusion matrix for building type classification with (a) Shallow Convolutional Neural Network (SCNN) and (b) Xception network.

all classes, the F1 scores improved with Xception, compared with the SCNN model, although for huts, barns, and farmhouses either precision or recall was higher for the SCNN model. The low support numbers for the greenhouse, industrial, and hospitality building classes have an unequal impact on their results. Despite the small training sample, recognition of greenhouses is successful with both CNNs. In contrast, industrial and hospitality buildings have particularly low precision scores.

The normalized confusion matrix (Fig. 4) displays the generally good classification with high recall scores on the diagonal and highlights which building types are most confused with each other off-diagonal. Most notably, the models mistake actual barns for alpine huts (24 % with SCNN, 19 % with Xception) and vice-versa, the Xception model in particular confuses 13 % of actual alpine huts with barns. Falsely classified are as well industrial buildings as garages in 16 % of the cases with SCNN and 13 % with Xception. Another pair of classes that is regularly misclassified are residential buildings and farmhouses. The SCNN model predicts farmhouses for 23 % of the residential buildings and the Xception model in 12 % of the cases. Furthermore, around 10 % of livestock buildings are mistaken for garages and part of industrial buildings, especially with SCNN, are classified as livestock buildings. Other pairs of building types have no particularly elevated misclassification rate (< 10 %).

The Xception model offers improvements over the SCNN for most error rates. Hospitality buildings misclassified as farms (−14 %), residential buildings misclassified as farms (−11 %), and industrial buildings misclassified as livestock buildings (−10 %) improve the most.

3.3. Comparison of impervious land mapping with Swiss Land Use Statistic

The results from the overlay between the impervious land use map produced in this study with Xception and Swiss Land Use Statistics indicate that a mere 11 % of the impervious land use area falls within grid cells of 100 $m \times 100$ m with matching land cover types. All land use classes exhibit an asymmetric distribution with respect to land cover class disagreement, with the exception of airfields and quarries and landfill sites, as depicted in Fig. 5. Only 5 % of the residential building area is located within raster cells classified as buildings in the Swiss Land Use Statistics, and all the residential building areas have a low raster overlay, i.e., that <20 % of the raster cells are covered by building area. Generally, larger buildings, such as agricultural and industrial buildings, exhibit a higher land cover agreement (10 % and 14 %, respectively) with some showing a high raster overlay (1 % and 7 %). Not surprisingly, distributions of surfaces around buildings within Swiss Land Use Statistics' raster cells are very similar to that of buildings.

Most road and railway areas are located within different land cover raster cells of the Swiss Land Use Statistics, at 92 % and 83 %, respectively. Railways exhibit a higher raster overlay, both in land cover agreeing raster cells (10 %) and in raster cells with other land cover types (14 %). Conversely, airfields as well as quarries and landfill sites, which have fewer linear land use patterns, have a more symmetrical distribution, with 29 % and 53 % of the area falling within corresponding land cover pixels, respectively. Simultaneously, they also have a high raster overlay.

Despite this major spatial discrepancy between this study's impervious land cover map and the raster-based Swiss Land Use Statistics, the raster grid's spatial resolution compensates for the discrepancy in terms of land use area within the study area. Fig. 5 illustrates the differences in land use areas between this study and the Swiss Land Use Statistics. Building areas are overestimated by the Swiss Land Use Statistics by a total of 4.2 km^2 and the surfaces around buildings are also larger by 8.3 km^2 compared with the mapping in this study. In contrast, transport infrastructure is underestimated by 12.7 km^2, primarily due to a difference of 12.8 km^2 in road areas. The high land cover class agreement and high raster overlay of quarries and landfill sites are also reflected in the total area, with a difference of only 0.4 km^2.

4. Discussion

4.1. Characterization of impervious land in rural regions

Impervious land cover in rural regions, comprising 1.9 % (113.2 km^2) of the study area, is in the same order of magnitude as impervious land cover in urban regions 2.6 % (154.6 km^2). Altogether, sealed surfaces amount to 4.5 % (267.8 km^2) of the Canton of Bern (5,959 km^2),

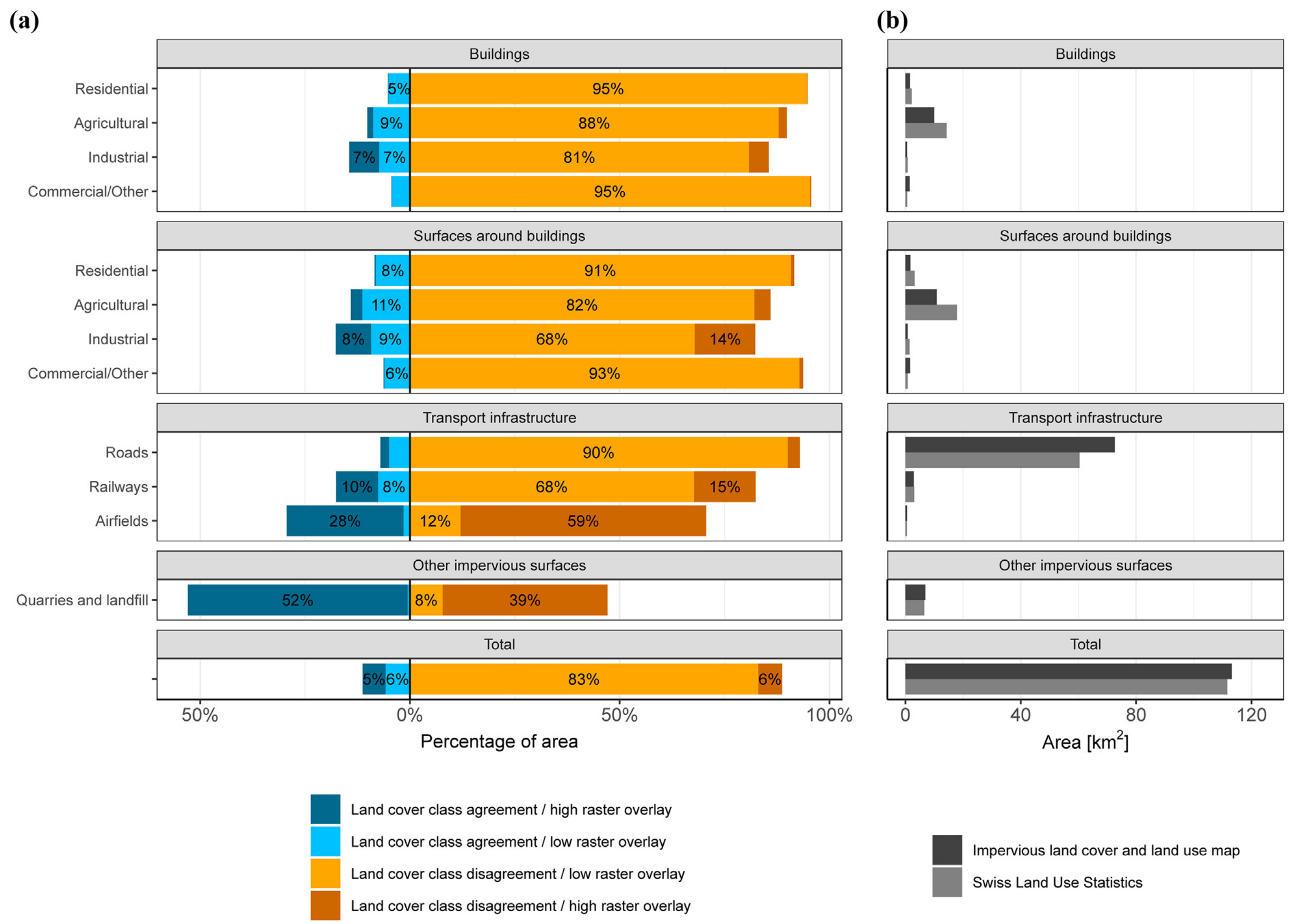

Fig. 5. (a) Distribution of impervious land use area in the raster cells of the Swiss Land Use Statistics by land cover class agreement and raster overlay (high if >20 % of the raster cell is covered by the impervious land cover identified in this study; low otherwise). (b) Total area of impervious land use area in the study area for reference according to the impervious land cover and land use map generated in this study as well as the Swiss Land Use Statistics.

of which 91 % (5,404 km^2) are rural regions and 9 % (555 km^2) urban regions. The comparison with urban regions underlines the importance of impervious surfaces in rural regions, which is overlooked in most studies on soil sealing, mostly because these building and infrastructure surfaces are typically not recognizable in coarser spatial data (Wang and Li, 2019). For reference, the land cover product of imperviousness density of the European Union's Copernicus Land Monitoring Service, with a 10-m raster, yields 3.0 % (179.2 km^2) of the study area, with a mere 0.5 % (30.72 km^2) of sealed surfaces in the rural regions and 2.5 % (148.5 km^2) in the urban regions. The minimal discrepancy in impervious surfaces in urban regions between our data and the CLMS product affirms our approach's efficacy. Other researchers similarly have used a combination of vector data and high-resolution aerial imagery to map impervious surfaces in cities (Schmidt and Barron, 2020) or, conversely, to assess urban green infrastructure (Codemo et al., 2022), but never in the context of imperviousness in rural landscapes.

Impervious land cover differs considerably between rural and urban regions. Rural regions contain 60 % of the total transport infrastructure within the study area, while urban regions account for the remaining 40 %. In contrast, the building area in rural regions is much smaller than in urban regions, at just 21 % of the total building footprints. In both rural and urban regions, impervious surfaces around buildings are equally important as the respective building area emphasizing the importance of their inclusion in impervious land cover mapping. Inevitably, using the NDVI index to analyze impervious surfaces around buildings can lead to certain under- or overestimations. In particular, bare soil and dry vegetation around livestock buildings are misclassified as impervious. Despite some inaccuracies in the analysis of impervious surfaces, this is limited to the buffered area around buildings. Other impervious surfaces, such as quarries and landfill sites, are mainly found in rural regions with 6.9 km^2 compared to 1.1 km^2 in urban regions. Furthermore, we found that impervious surfaces in rural regions have other impervious land uses with buildings designed for highly different purposes (cf. Kang et al., 2018).

Buildings with agricultural uses (farmhouses, livestock buildings, greenhouses, barns, and alpine huts) add up to 8.5 km^2 and represent 61 % of the building area in rural regions. These buildings serve crucial functions in supporting agricultural activities, including providing living space, sheltering livestock, and storing farm machinery. In contrast, residential buildings comprise only 12 % of the built area, and even less is accounted for by industrial, hospitality, and other buildings. The distribution of building type area is largely due to strict regulations on building outside of building zones in Switzerland, where agricultural buildings can be approved in accordance with zoning regulations, and other uses are subject to exemptions for existing buildings or site-specific new construction. In this context, changes in socioeconomic conditions notably can exert various effects on buildings in rural regions. For instance, farm growth and intensification of livestock farming require larger livestock buildings, while farmland abandonment, often seen in mountainous regions (Lasanta et al., 2017), has been demonstrated to foster the conversion of farmhouses to purely residential use (van der Vaart, 2005). Moreover, diversification through recreational and tourism services can take advantage of unused barns or alpine cabins and enhance commercial use in rural regions (Sardaro et al., 2021). Our accurate mapping of impervious land cover and land use can be a valuable resource for examining urbanization processes in rural regions further.

The comparison between impervious land use mapped in this study and raster-based Swiss Land Use Statistics shows that vast spatial differences exist at the medium spatial resolution of 100 m. Yet, on a larger scale, total areas of land uses are comparable, especially when aggregating categories, as also shown by other authors (Grêt-Regamey et al., 2014). By interpreting the land cover/land use value at the center point of a raster cell, the Swiss Land Use Statistics can capture small-scale impervious land uses in rural regions, but overlay with the corresponding land use class is small in the dispersed arrangement of rural regions. Planar structures such as buildings and impervious surfaces around buildings, generally are overestimated by the raster-based dataset, and linear structures, such as roads, are underestimated. While we are aware that data collection times do not match exactly, the annual impervious land cover change rate of the Swiss Land Use Statistics in the rural regions is in a negligible order of 0.5 % (ARE, 2023). The spatial disagreement between this study's land use map and the raster-based Swiss Land Use Statistics poses important implications for land cover and land use monitoring when monitoring impervious land on local and regional scales, highlighting the relevance of a high spatial resolution. This finding is consistent with van Vliet et al. (2019), who observed that much of the impervious land is distributed in small fractions within otherwise pervious land pixels of 1 km^2 and that impervious land expansion occurs in small incremental steps undiscovered by pixel classification.

4.2. Building type classification

The overall accuracy and weighted F1 score of 79 % each (with the Xception model) for the building classification with CNN is in line with similar research in this field. Yet, a notable difference is that land use classification in urban regions is often based on patterns that consist of multiple buildings and roads included in a pixel or a scene (Albert et al., 2017; Rosier et al., 2022), while the classification in rural regions typically is based only on features of a single building. Kang et al. (2018) achieved an F1 score of 58 % in classifying apartments, churches, garages, houses, retail buildings, etc. with street view images using state-of-the-art deep CNN architectures, and Hoffmann et al. (2019) reached 75 % in classifying commercial, industrial, public, and residential buildings by fine-tuning fusion strategies with CNNs to combine aerial and street view imagery. The deep neural network Xception improved the classification of building types compared with the SCNN in all evaluation metrics, indicating that crucial high-level features are recognized. Similar pairs of building types, e.g., residential buildings and farmhouses, which share recognizable features such as gardens, patios, trampolines, etc., are better distinguished presumably because the model understands more semantically meaningful scenes, e.g., the composition of residential features with hay bales, light inlets, animals, etc., clearly indicating farmhouse. Surprisingly good results were obtained for building types with small class support size (greenhouses, industrial buildings, commercial buildings). Greenhouses in particular were classified with high accuracy due to their distinct appearance. Another implication of the rather small overall size of the training sample was overfitting, which occurred primarily with Xception, indicating that the model's complexity became too high, and it began to learn noise in the training data. Despite regularization through data augmentation and dropout layers, an early stop was necessary to achieve accurate results.

Clearly, accurate building type classification with CNN is limited to buildings whose use is visually recognizable from an aerial view. Distinct architectural features, roof structures, and surrounding elements and objects differentiate the use of buildings. For certain building types, i.e., hospitality or industrial buildings, physical appearance is less distinct for an effective recognition within this study's training sample. Integrating geospatial big data (e.g., census or social media data) could be an effective way to combine the physical and socioeconomic aspects and enhance the impervious land use classification at the individual building level beyond what is visually recognizable (Yin et al., 2021). Related to this limitation is the question of transferability of the neural network model to other regions. Given the differences in unique local architectural styles, such as for farmhouses in Switzerland, the approach would require a region-specific sample to train the model. The addition of socioeconomic data could also improve transferability (Rosier et al., 2022).

4.3. Limitations of data availability and generalizability of the methodology

We acknowledge several limitations of our study related to data availability and the generalizability of our methodology. Our research benefits from precise and complete vector data, which may not be available in all parts of the world. As an alternative data source, building footprints and transport infrastructure could be extracted from the free OpenStreetMap (OSM). Studies have found high accuracy and completeness of volunteered geographic information for the street network (Barrington-Leigh and Millard-Ball, 2017); however, the completeness of building footprints may vary drastically depending on the region (Müller et al., 2015; Tian et al., 2019; Wang et al., 2020; Zhou et al., 2022). Therefore, an assessment of data completeness is essential when using OSM (Brovelli and Zamboni, 2018; Hecht et al., 2013). Another alternative is the use of object-based image analysis (OBIA) of high-resolution remote sensing imagery for the generation of vector-based impervious land cover maps (Blaschke, 2010; Hoeser and Kuenzer, 2020). While great advancements have been made, and numerous capable OBIA algorithms exist, they are computationally expensive (Hossain and Chen, 2019) and require an accuracy assessment, which is further complicated by the difficulty of obtaining validation data (Wulder et al., 2018). Moreover, authoritative geospatial data is increasingly collected and published with open data licenses (Coetzee et al., 2020). For instance, buildings, transport infrastructure, and cadastral parcels are part of the European Directive "Infrastructure for Spatial Information in Europe (INSPIRE)" (European Parliament and Council, 2007), which aims to create a pan-European spatial data infrastructure and recognizes the importance of usability, interoperability, and accessibility. However, these efforts have yet to achieve global coverage. Thus, while the methodology we propose is generalizable for use in various regions, its application may be constrained by the availability and quality of local data.

Overall, this study's results show the importance of impervious soils in rural regions, and that transport infrastructure and agricultural land use predominate impervious land cover in rural regions. Although the findings may not be representative of all rural contexts with varying socioeconomic, environmental, and structural characteristics, the challenges associated with large impervious land uses reflect broader trends in increasing traffic outside of urban areas (van Strien and Grêt-Regamey, 2024) and ongoing structural change in agriculture (Neuenfeldt et al., 2019). Knowledge on the extent and use of impervious surfaces can help formulate sustainable goals and policies for managing land resources and protecting rural landscapes. An integrated approach to policy making recognizes the underlying driving forces for effective steering and stabilization of soil sealing. Therefore, future research should target processes and investigate drivers that effectively underlie the process of soil sealing in rural regions, in which the impervious surface map of this study can serve as a foundation.

5. Conclusions

Our research aimed to characterize impervious land use in rural regions by combining precise authoritative vector data with very-high-resolution remote sensing imagery. The results revealed that while the composition of impervious surfaces varies, the total area of impervious surfaces in rural regions is almost as large as in urban regions, albeit distributed over a much larger area. We utilized CNN architectures to determine land use of impervious surfaces at the level of individual buildings with good performance. This first-of-its-kind characterization of impervious surfaces in rural regions demonstrates that transport infrastructure and buildings used for agriculture and livestock represent the most important socioeconomic use of impervious land in rural regions. Urban containment strategies, currently concerned primarily with controlling peri-urbanization, must address these prevalent impervious land uses. Additionally, our comparison with raster-based land use data revealed striking spatial differences in rural regions' small-scale structures, although the sum of total areas remained surprisingly similar. These findings contribute to a better understanding of impervious land use patterns and can help examine the processes leading to soil sealing in rural regions. As a support for spatial planners, impervious land use maps can improve effective land allocation and contribute to sustainable land management.

Declaration of competing interests

The authors declare that they have no known competing financial interests or personal relationships that could have appeared to influence the work reported in this paper.

CRediT authorship contribution statement

Andreas Moser: Writing – original draft, Visualization, Software, Methodology, Investigation, Formal analysis, Data curation, Conceptualization. **Jasper van Vliet:** Conceptualization, Writing – review & editing, Supervision. **Ulrike Wissen Hayek:** Supervision, Project administration. **Adrienne Grêt-Regamey:** Writing – review & editing, Supervision, Funding acquisition, Conceptualization, Project administration.

Acknowledgements

This research is part of the project "Interkantonal koordiniertes Monitoring Bauen ausserhalb Bauzonen" and was funded by the Swiss Federal Office for Spatial Development (ARE), Swiss Federal Office for Environment (FOEN), Swiss Federal Office for Agriculture (FOAG), Canton of Bern (Amt für Gemeinden und Raumordnung), Canton of St. Gallen (Amt für Raumentwicklung und Geoinformation), Canton of Appenzell Ausserrhoden (Amt für Raum und Wald), Canton of Appenzell Innerrhoden (Amt für Raumentwicklung), Canton of Glarus (Abteilung Raumentwicklung und Geoinformation), and Canton of Vaud (Direction générale du territoire et du logement). JvV was supported by the Netherlands Organization for Scientific Research NWO in the form of a VIDI grant (Grant No. VI.Vidi.198.008).

Supplementary materials

Supplementary material associated with this article can be found in the online version, at doi:10.1016/j.geosus.2024.08.004.

References

Albert, A., Kaur, J., Gonzalez, M.C., 2017. Using convolutional networks and satellite imagery to identify patterns in urban environments at a large scale. In: Proceedings of the 23rd ACM SIGKDD International Conference on Knowledge Discovery and Data Mining, Halifax. ACM, pp. 1357–1366. doi:10.1145/3097983.3098070.

Alzubaidi, L., Zhang, J., Humaidi, A.J., Al-Dujaili, A., Duan, Y., Al-Shamma, O., Santamaría, J., Fadhel, M.A., Al-Amidie, M., Farhan, L., 2021. Review of deep learning: concepts, CNN architectures, challenges, applications, future directions. J. Big Data 8 (1), 53. doi:10.1186/s40537-021-00444-8.

Antrop, M., 2000. Changing patterns in the urbanized countryside of Western Europe. Landsc. Ecol. 15, 257–270.

Antrop, M., 2004. Landscape change and the urbanization process in Europe. Landsc. Urban Plan. 67 (1–4), 9–26. doi:10.1016/S0169-2046(03)00026-4.

Barrington-Leigh, C., Millard-Ball, A., 2017. The world's user-generated road map is >80 % complete. PLoS One 12 (8), e0180698. doi:10.1371/journal.pone.0180698.

Baveye, P.C., Baveye, J., Gowdy, J., 2016. Soil "ecosystem" services and natural capital: critical appraisal of research on uncertain ground. Front. Environ. Sci. 4, 41. doi:10.3389/fenvs.2016.00041.

Blaschke, T., 2010. Object based image analysis for remote sensing. ISPRS J. Photogramm. Remote Sens. 65 (1), 2–16. doi:10.1016/j.isprsjprs.2009.06.004.

Brovelli, M., Zamboni, G., 2018. A new method for the assessment of spatial accuracy and completeness of OpenStreetMap building footprints. ISPRS J. Photogramm. Remote Sens. 7 (8), 289. doi:10.3390/ijgi7080289.

Chen, Y., Jiang, H., Li, C., Jia, X., Ghamisi, P., 2016. Deep feature extraction and classification of hyperspectral images based on convolutional neural networks. IEEE Trans. Geosci. Remote Sens. 54 (10), 6232–6251. doi:10.1109/TGRS.2016.2584107.

Chen, B., Tu, Y., Song, Y., Theobald, D.M., Zhang, T., Ren, Z., Li, X., Yang, J., Wang, J., Wang, X., Gong, P., Bai, Y., Xu, B., 2021. Mapping essential urban land use categories with open big data: results for five metropolitan areas in the United States of America. ISPRS J. Photogramm. Remote Sens. 178, 203–218. doi:10.1016/j.isprsjprs.2021.06.010.

Chollet, F., 2017. Xception: deep learning with depthwise separable convolutions. In: 2017 IEEE Conference on Computer Vision and Pattern Recognition (CVPR), Honolulu. IEEE, pp. 1800–1807. doi:10.1109/CVPR.2017.195.

Codemo, A., Pianegonda, A., Ciolli, M., Favargiotti, S., Albatici, R., 2022. Mapping pervious surfaces and canopy cover using high-resolution airborne imagery and digital elevation models to support urban planning. Sustainability 14 (10), 6149. doi:10.3390/su14106149.

Coetzee, S., Ivánová, I., Mitasova, H., Brovelli, M., 2020. Open geospatial software and data: a review of the current state and a perspective into the future. ISPRS Int. J. Geo-Inf. 9 (2), 90. doi:10.3390/ijgi9020090.

Copernicus Land Monitoring Service (CLMS), 2020. Copernicus Land Monitoring Service, European Environment Agency.

Defries, R.S., Townshend, J.R.G., 1994. NDVI-derived land cover classifications at a global scale. Int. J. Remote Sens. 15 (17), 3567–3586. doi:10.1080/01431169408954345.

European Commission, 2011. Roadmap to a Resource Efficient Europe (No. COM(2011) 571 Final) European Commission, Brussels (accessed 17 April 2023).

European Environment Agency (EEA), 2018. European Environment Agency.

European Environment Agency (EEA), 2020. Imperviousness and Imperviousness Change in Europe. European Environment Agency, Copenhagen (accessed 13 April 2023).

European Parliament and Council, 2007. Directive 2007/2/EC of the European Parliament and of the Council of 14 March 2007 establishing an Infrastructure for Spatial Information in the European Community (INSPIRE) (Official Journal of the European Union No. L 108/1). https://eur-lex.europa.eu/eli/dir/2007/2/oj (accessed 28 April 2023).

Eurostat, 1998. Classification of Types of Constructions (CC). European Commission, Luxembourg (accessed 29 March 2023).

Eurostat, 2022. Population density by NUTS 3 region (online data code: demo_r_d3dens).

Federal Office for Spatial Development (ARE), 2022. Bauzonenstatistik Schweiz 2022 – Statistik und Analysen. Federal Office for Spatial Development, Bern. (in German).

Federal Office for Spatial Development (ARE), 2023. Monitoring Bauen ausserhalb Bauzonen – Standbericht 2023. Federal Office for Spatial Development, Bern. (in German).

Federal Statistical Office (FSO), 2019. Arealstatistik Schweiz - Erhebung Der Bodennutzung und Der Bodenbedeckung (No. 897–1900). Federal Statistical Office, Neuchâtel. (in German).

Federal Statistical Office (FSO), 2022a. Federal Statistical Office https://www.bfs.admin.ch/asset/en/px-x-0102020000_201. (accessed 20 March 2023).

Federal Statistical Office (FSO), 2022b. Federal Statistical Office https://www.housing-stat.ch/de/index.html. (accessed 29 March 2023). (in German).

Géron, A., 2019. Hands-on Machine Learning With Scikit-Learn, Keras, and TensorFlow: Concepts, Tools, and Techniques to Build Intelligent Systems, 2nd ed. O'Reilly Media, Inc., Sebastopol.

Gao, J., O'Neill, B.C., 2020. Mapping global urban land for the 21st century with data-driven simulations and Shared Socioeconomic Pathways. Nat. Commun. 11 (1), 2302. doi:10.1038/s41467-020-15788-7.

Gerber, J.-D., Hartmann, T., Hengstermann, A., 2018. Instruments of Land Policy: Dealing with Scarcity of Land, 1st ed. Routledge, Abingdon doi:10.4324/9781315511658.

Grêt-Regamey, A., Weibel, B., Bagstad, K.J., Ferrari, M., Geneletti, D., Klug, H., Schirpke, U., Tappeiner, U., 2014. On the effects of scale for ecosystem services mapping. PLoS One 9 (12), e112601. doi:10.1371/journal.pone.0112601.

He, K., Zhang, X., Ren, S., Sun, J., 2016. Deep residual learning for image recognition. In: 2016 IEEE Conference on Computer Vision and Pattern Recognition (CVPR), Las Vegas. IEEE, pp. 770–778. doi:10.1109/CVPR.2016.90.

Hecht, R., Kunze, C., Hahmann, S., 2013. Measuring completeness of building footprints in OpenStreetMap over space and time. ISPRS Int. J. Geo-Inf. 2 (4), 1066–1091. doi:10.3390/ijgi2041066.

Hennig, E.I., Schwick, C., Soukup, T., Orlitová, E., Kienast, F., Jaeger, J.A.G., 2015. Multi-scale analysis of urban sprawl in Europe: towards a European de-sprawling strategy. Land Use Policy 49, 483–498. doi:10.1016/j.landusepol.2015.08.001.

Hersperger, A.M., Oliveira, E., Pagliarin, S., Palka, G., Verburg, P., Bolliger, J., Grădinaru, S., 2018. Urban land-use change: the role of strategic spatial planning. Glob. Environ. Change 51, 32–42. doi:10.1016/j.gloenvcha.2018.05.001.

Hoeser, T., Kuenzer, C., 2020. Object detection and image segmentation with deep learning on Earth observation data: a review-Part I: evolution and recent trends. Remote. Sens. 12, 1667. doi:10.3390/rs12101667.

Hoffmann, E.J., Wang, Y., Werner, M., Kang, J., Zhu, X.X., 2019. Model fusion for building type classification from aerial and street view images. Remote. Sens. 11 (11), 1259. doi:10.3390/rs11111259.

Hossain, M.D., Chen, D., 2019. Segmentation for object-based image analysis (OBIA): a review of algorithms and challenges from remote sensing perspective. ISPRS J. Photogramm. Remote Sens. 150, 115–134. doi:10.1016/j.isprsjprs.2019.02.009.
Ioffe, S., Szegedy, C., 2015. Batch normalization: accelerating deep network training by reducing internal covariate shift. In: Proceedings of the 32nd International Conference on Machine Learning, Proceedings of Machine Learning Research. PMLR, Lille, pp. 448–456.
Kang, J., Körner, M., Wang, Y., Taubenböck, H., Zhu, X.X., 2018. Building instance classification using street view images. ISPRS J. Photogramm. Remote Sens. 145, 44–59. doi:10.1016/j.isprsjprs.2018.02.006.
Kim, B., Yuvaraj, N., Sri Preethaa, K.R., Arun Pandian, R., 2021. Surface crack detection using deep learning with shallow CNN architecture for enhanced computation. Neural Comput. Appl. 33 (15), 9289–9305. doi:10.1007/s00521-021-05690-8.
Kingma, D.P., Ba, J., 2014. Adam: a method for stochastic optimization. arXiv preprint. http://arxiv.org/abs/1412.6980.
Konferenz der Kantonalen Vermessungsämter (KKVA), 2011. Detaillierungsgrad in der amtlichen Vermessung - Informationsebene Bodenbedeckung. Konferenz der Kantonalen Vermessungsämter, swisstopo/Eidgenössische Vermessungsdirektion. https://www.cadastre.ch/content/cadastre-internet/de/manual-av/publication/guidline.download/cadastre-internet/de/documents/av-richtlinien/Richtlinie-Detaillierungsgrad-BB-de.pdf. (accessed 26 September 2022) (in German).
Krizhevsky, A., Sutskever, I., Hinton, G.E., 2012. ImageNet classification with deep convolutional neural networks. Commun. ACM, 60, pp. 84–90.
Lal, R., Bouma, J., Brevik, E., Dawson, L., Field, D.J., Glaser, B., Hatano, R., Hartemink, A.E., Kosaki, T., Lascelles, B., Monger, C., Muggler, C., Ndzana, G.M., Norra, S., Pan, X., Paradelo, R., Reyes-Sánchez, L.B., Sandén, T., Singh, B.R., Spiegel, H., Yanai, J., Zhang, J., 2021. Soils and sustainable development goals of the United Nations: an International Union of Soil Sciences perspective. Geoderma Reg. 25, e00398. doi:10.1016/j.geodrs.2021.e00398.
Lasanta, T., Arnáez, J., Pascual, N., Ruiz-Flaño, P., Errea, M.P., Lana-Renault, N., 2017. Space–time process and drivers of land abandonment in Europe. Catena 149, 810–823. doi:10.1016/j.catena.2016.02.024.
Lei, F., Liu, X., Dai, Q., Ling, B.W.-K., 2020. Shallow convolutional neural network for image classification. SN Appl. Sci. 2 (1), 97. doi:10.1007/s42452-019-1903-4.
Li, W., Dong, R., Fu, H., Wang, J., Yu, L., Gong, P., 2020. Integrating Google Earth imagery with Landsat data to improve 30-m resolution land cover mapping. Remote Sens. Environ. 237, 111563. doi:10.1016/j.rse.2019.111563.
Liu, X., Hu, G., Chen, Y., Li, X., Xu, X., Li, S., Pei, F., Wang, S., 2018. High-resolution multi-temporal mapping of global urban land using Landsat images based on the Google Earth Engine Platform. Remote Sens. Environ. 209, 227–239. doi:10.1016/j.rse.2018.02.055.
Liu, X., Huang, Y., Xu, X., Li, X., Li, X., Ciais, P., Lin, P., Gong, K., Ziegler, A.D., Chen, A., Gong, P., Chen, J., Hu, G., Chen, Y., Wang, S., Wu, Q., Huang, K., Estes, L., Zeng, Z., 2020. High-spatiotemporal-resolution mapping of global urban change from 1985 to 2015. Nat. Sustain. 3 (7), 564–570. doi:10.1038/s41893-020-0521-x.
Müller, F., Iosifescu, I., Hurni, L., 2015. Assessment and visualization of OSM building footprint quality. In: Proceedings of the 27th International Cartographic Conference (ICC 2015). Rio de Janeiro.
Ma, L., Liu, Y., Zhang, X., Ye, Y., Yin, G., Johnson, B.A., 2019. Deep learning in remote sensing applications: a meta-analysis and review. ISPRS J. Photogramm. Remote Sens. 152, 166–177. doi:10.1016/j.isprsjprs.2019.04.015.
McDonnell, M.D., Vladusich, T., 2015. Enhanced image classification with a fast-learning shallow convolutional neural network. In: 2015 International Joint Conference on Neural Networks (IJCNN), Killarney. IEEE, pp. 1–7. doi:10.1109/IJCNN.2015.7280796.
Miao, S., Xu, H., Han, Z., Zhu, Y., 2019. Recognizing facial expressions using a shallow convolutional neural network. IEEE Access 7, 78000–78011. doi:10.1109/ACCESS.2019.2921220.
Neuenfeldt, S., Gocht, A., Heckelei, T., Ciaian, P., 2019. Explaining farm structural change in the European agriculture: a novel analytical framework. Eur. Rev. Agric. Econ. 46 (5), 713–768. doi:10.1093/erae/jby037.
Peroni, F., Pappalardo, S.E., Facchinelli, F., Crescini, E., Munafò, M., Hodgson, M.E., De Marchi, M., 2022. How to map soil sealing, land take and impervious surfaces? A systematic review. Environ. Res. Lett. 17 (5), 053005. doi:10.1088/1748-9326/ac6887.
Pesaresi, M., Ehrlich, D., Ferri, S., Florczyk, A., Freire, S., Halkia, M., Julea, A., Kemper, T., Soille, P., Syrris, V., 2016. Operating procedure for the production of the global human settlement layer from Landsat data of the epochs 1975, 1990, 2000, and 2014 (JRC Technical Report No. EUR 27741). European Union, Luxembourg doi:10.2788/253582.
Ravetz, J., Fertner, C., Nielsen, T.S., 2013. The dynamics of peri-urbanization. In: Nilsson, K., Pauleit, S., Bell, S., Aalbers, C., Sick Nielsen, T.A. (Eds.), Peri-Urban Futures: Scenarios and Models for Land Use Change in Europe. Springer, Berlin, Heidelberg, pp. 13–44. doi:10.1007/978-3-642-30529-0_2.
Rosier, J.F., Taubenböck, H., Verburg, P.H., van Vliet, J., 2022. Fusing Earth observation and socioeconomic data to increase the transferability of large-scale urban land use classification. Remote Sens. Environ. 278, 113076. doi:10.1016/j.rse.2022.113076.
Sardaro, R., La Sala, P., De Pascale, G., Faccilongo, N., 2021. The conservation of cultural heritage in rural areas: stakeholder preferences regarding historical rural buildings in Apulia, southern Italy. Land Use Policy 109, 105662. doi:10.1016/j.landusepol.2021.105662.
Scalenghe, R., Marsan, F.A., 2009. The anthropogenic sealing of soils in urban areas. Landsc. Urban Plan. 90 (1–2), 1–10. doi:10.1016/j.landurbplan.2008.10.011.
Schmidt, S., Barron, C., 2020. Mapping impervious surfaces precisely—a GIS-based methodology combining vector data and high-resolution airborne imagery. J. Geovis. Spat. Anal. 4 (1), 14. doi:10.1007/s41651-020-00055-6.
Shaw, B.J., Van Vliet, J., Verburg, P.H., 2020. The peri-urbanization of Europe: a systematic review of a multifaceted process. Landsc. Urban Plan. 196, 103733. doi:10.1016/j.landurbplan.2019.103733.
Simonyan, K., Zisserman, A., 2014. Very deep convolutional networks for large-scale image recognition. arXiv preprint. arXiv:1409.1556.
Srivastava, S., Vargas Muñoz, J.E., Lobry, S., Tuia, D., 2020. Fine-grained landuse characterization using ground-based pictures: a deep learning solution based on globally available data. Int. J. Geogr. Inf. Sci. 34 (6), 1117–1136. doi:10.1080/13658816.2018.1542698.
Stolte, J., Tesfai, M., Øygarden, L., Kværnø, S., Keizer, J., Verheijen, F., Panagos, P., Ballabio, C., Hessel, R., 2015. Soil Threats in Europe (JRC Technical Report No. EUR 27607 EN). European Union, Luxembourg doi:10.2788/828742.
Swiss Federal Act on Spatial Planning, 1979. https://www.fedlex.admin.ch/eli/cc/1979/1573_1573_1573/en (accessed 12 July 2023).
swisstopo, 2021a. SWISSIMAGE 10 cm. Federal Office of Topography swisstopo, Bern (accessed 29 March 2023).
swisstopo, 2021b. SWISSIMAGE RS. Federal Office of Topography swisstopo, Bern (accessed 29 March 2023).
Szegedy, C., Liu, W., Jia, Y.Q., Sermanet, P., Reed, S., Anguelov, D., Erhan, D., Vanhoucke, V., Rabinovich, A., 2015. Going deeper with convolutions. In: 2015 IEEE Conference on Computer Vision and Pattern Recognition (CVPR), Boston. IEEE, pp. 1–9. doi:10.1109/CVPR.2015.7298594.
Szegedy, C., Ioffe, S., Vanhoucke, V., Alemi, A., 2017. Inception-v4, Inception-ResNet and the impact of residual connections on learning. In: Proceedings of the Thirty-First AAAI Conference on Artificial Intelligence (AAAI-17), San Francisco, pp. 4278–4284. doi:10.1609/aaai.v31i1.11231.
Taylor, L., Nitschke, G., 2018. Improving deep learning with generic data augmentation. In: 2018 IEEE Symposium Series on Computational Intelligence (SSCI), Bangalore, pp. 1542–1547. doi:10.1109/SSCI.2018.8628742.
Tian, Y., Zhou, Q., Fu, X., 2019. An analysis of the evolution, completeness and spatial patterns of OpenStreetMap building data in China. ISPRS Int. J. Geo-Inf. 8 (1), 35. doi:10.3390/ijgi8010035.
UN General Assembly, 2015. Transforming our world: the 2030 agenda for sustainable development (No. A/RES/70/1). https://www.refworld.org/legal/resolution/unga/2015/en/111816 (accessed 9 July 2024).
van der Vaart, J.H.P., 2005. Towards a new rural landscape: consequences of non-agricultural re-use of redundant farm buildings in Friesland. Landsc. Urban Plan. 70 (1–2), 143–152. doi:10.1016/j.landurbplan.2003.10.010.
van Rijsbergen, C.J., 1979. Information Retrieval, 2nd ed. Butterworth-Heinemann, Oxford.
van Strien, M.J., Grêt-Regamey, A., 2024. A global time series of traffic volumes on extra-urban roads. Sci. Data 11 (1), 470. doi:10.1038/s41597-024-03287-z.
van Vliet, J., Verburg, P.H., Grădinaru, S.R., Hersperger, A.M., 2019. Beyond the urban-rural dichotomy: towards a more nuanced analysis of changes in built-up land. Comput. Environ. Urban Syst. 74, 41–49. doi:10.1016/j.compenvurbsys.2018.12.002.
Wang, Y., Li, M., 2019. Urban impervious surface detection from remote sensing images: a review of the methods and challenges. IEEE Geosci. Remote Sens. Mag. 7 (3), 64–93. doi:10.1109/MGRS.2019.2927260.
Wang, S., Zhou, Q., Tian, Y., 2020. Understanding completeness and diversity patterns of OSM-based land-use and land-cover dataset in China. ISPRS Int. J. Geo-Inf. 9 (9), 531. doi:10.3390/ijgi9090531.
Weng, Q., 2012. Remote sensing of impervious surfaces in the urban areas: requirements, methods, and trends. Remote Sens. Environ. 117, 34–49. doi:10.1016/j.rse.2011.02.030.
Wulder, M.A., Coops, N.C., Roy, D.P., White, J.C., Hermosilla, T., 2018. Land cover 2.0. Int. J. Remote Sens. 39 (12), 4254–4284. doi:10.1080/01431161.2018.1452075.
Yin, J., Dong, J., Hamm, N.A.S., Li, Z., Wang, J., Xing, H., Fu, P., 2021. Integrating remote sensing and geospatial big data for urban land use mapping: a review. Int. J. Appl. Earth Obs. Geoinf. 103, 102514. doi:10.1016/j.jag.2021.102514.
Yoo, S., Lee, J., Gholami Farkoushi, M., Lee, E., Sohn, H.-G., 2022. Automatic generation of land use maps using aerial orthoimages and building floor data with a Conv-Depth Block (CDB) ResU-Net architecture. Int. J. Appl. Earth Obs. Geoinf. 107, 102678. doi:10.1016/j.jag.2022.102678.
Yue, J., Zhao, W., Mao, S., Liu, H., 2015. Spectral–spatial classification of hyperspectral images using deep convolutional neural networks. Remote Sens. Lett. 6 (6), 468–477. doi:10.1080/2150704X.2015.1047045.
Zhang, C., Sargent, I., Pan, X., Li, H., Gardiner, A., Hare, J., Atkinson, P.M., 2018. An object-based convolutional neural network (OCNN) for urban land use classification. Remote Sens. Environ. 216, 57–70. doi:10.1016/j.rse.2018.06.034.
Zhao, W., Du, S., Emery, W.J., 2017. Object-based convolutional neural network for high-resolution imagery classification. IEEE J. Sel. Top. Appl. Earth Obs. Remote Sens. 10 (7), 3386–3396. doi:10.1109/JSTARS.2017.2680324.
Zhou, Q., Wang, S., Liu, Y., 2022. Exploring the accuracy and completeness patterns of global land-cover/land-use data in OpenStreetMap. Appl. Geogr. 145, 102742. doi:10.1016/j.apgeog.2022.102742.
Zhu, X.X., Tuia, D., Mou, L., Xia, G.-S., Zhang, L., Xu, F., Fraundorfer, F., 2017. Deep learning in remote sensing: a comprehensive review and list of resources. IEEE Geosci. Remote Sens. Mag. 5 (4), 8–36. doi:10.1109/MGRS.2017.27623.